Proceedings of the Second International Conference on Press-in Engineering 2021, Kochi, Japan – Matsumoto et al (eds)

Design considerations for piles jacked or driven into strong soil or weak rock

(IPA 15th Anniversary Special Keynote Lecture)

M.F. Randolph
The University of Western Australia

ABSTRACT: Piles are often used in weathered soil profiles, perhaps needing to be embedded down to a hard, less weathered zone. The weathered material may vary from a strong soil to weak rock, often comprising a mix of partially weathered blocks embedded in a soil matrix. These are difficult materials for estimation of design parameters but may also cause problems during the installation of jacked or driven piles. The paper first reviews some of the design approaches for estimating engineering parameters such as shaft friction and end-bearing in these types of soil and weak rock. It then discusses the potential for pile tip damage during the installation process, presenting preliminary results from current doctoral research to assess conditions for pile tip damage more accurately.

1 INTRODUCTION

Although cast-in-situ piles such as rock sockets are the most common type of pile used in weak to moderate strength rock, jacked or driven piles also have a place, particularly in variably weathered profiles. There are, however, significant design challenges, ranging from characterization of the strength of weak rock and the associated design parameters to the risks of premature refusal on less weathered layer or of damage to the pile tip as it is penetrated through the layers.

Open-ended pipe piles are the most frequent pile type for coastal developments such as wharves and, increasingly, the large diameter monopiles used to support offshore wind turbines.

This paper reviews design approaches for jacked and driven piles in strong soil and soft rock, including characterization of the mass strength of the soil and correlations proposed in the literature for key engineering parameters such as shaft friction and end-bearing resistance. This material draws on the discussion in Randolph (2019).

In the second half of the paper, application of steel pipe piles for offshore wind turbines is considered, in particular the risk of tip damage as such relatively thin-walled piles are penetrated through the soil and rock profile. Current doctoral research by Juliano Nietiedt at the University of Western Australia has been addressing this problem with the objective of developing quantitative design guidelines for potential tip damage and the propagation of a mild dent into severe deformation.

2 CHARACTERIZATION OF ROCK

2.1 *Penetrometer correlations for weak rock*

In weak rock, it is possible to use conventional cone penetrometer tests (CPTs) in addition to taking samples and testing them in the laboratory. This provides a transition from strong soil to weak rock, allowing correlations to be developed as has been undertaken for calcareous sediments such as calcarenite (or weak limestone) and chalk.

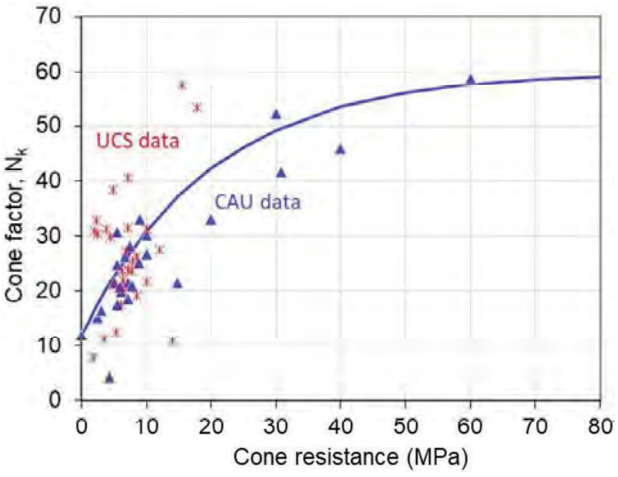

Figure 1. Correlation of cone factor with cone resistance.

Correlations relate the cone resistance q_{CPT} and rock shear strength ($s_u = q_{ucs}/2$) via a cone factor N_k,

DOI: 10.1201/9781003215226-63

just as for clays, where q_{ucs} is the unconfined compression strength or equivalent failure stress applied under triaxial conditions. Figure 1 shows one such correlation, where a reasonable fit to the data is obtained using an exponential increase in N_k with increasing cone resistance, according to

$$N_k = N_{k,\max} - \left(N_{k,\max} - N_{k,\min}\right)e^{-0.005 q_{CPT}/p_a} \quad (1)$$

taking $N_{k,min}$ as 12 and $N_{k,max}$ as 60 (with p_a standing for atmospheric pressure of 0.1 MPa).

The increase of N_k with cone resistance arises partly because of an increase in the ratio of rock mass strength to unconfined compression strength as the quality of the rock increases, as discussed below, but also because of increasingly partially drained conditions during penetration of the cone.

2.2 *Mass rock properties for design*

Characterizing the strength of and how it responds during failure (i.e. whether exhibiting brittle fracture or merely compressing into a rubble) is extremely challenging. Different failure modes will depend on the degree of confinement, and even on the progress of a particular load application, such as the response in bearing beneath the base of a pile.

The unconfined compression strength (UCS) test is one of the most common forms of laboratory strength measurement for rock, with the deviatoric strength at failure referred to here as q_{ucs}. The UCS may be 'extended' to a non-linear failure envelope using models such as that developed by Hoek and Brown (Hoek & Brown 1997, Hoek et al. 2002).

The Hoek-Brown failure envelope is expressed as

$$\sigma'_1 = \sigma'_3 + \sigma_{ci}\left(m_b \frac{\sigma'_3}{\sigma_{ci}} + s\right)^a \quad (2)$$

where σ_{ci} is the UCS for intact (undamaged) rock. In high quality rock this becomes equivalent to q_{ucs}, assuming that the laboratory unconfined strength test is carried out on intact, undamaged, rock. In general, however, σ_{ci} exceeds q_{ucs} due to the presence of internal weaknesses in the sample.

Hoek et al. (2002) correlated the various parameters in Eq. (2) to the geological strength index (*GSI*) according to

$$\begin{aligned} m_b &= m_i \exp\left(\frac{GSI - 100}{28 - 14D}\right) \\ s &= \exp\left(\frac{GSI - 100}{9 - 3D}\right) \\ a &= 0.5 + \left[\mathrm{e}^{-GSI/15} - \mathrm{e}^{-100/15}\right]/6 \sim 0.5 \end{aligned} \quad (3)$$

where D is a damage factor (0 undamaged to 1 completely fractured) due to blasting or other form of excavation, and m_i is the material constant for the rock in question.

The geological strength index itself is a rather subjective parameter based on the joint spacing (*RQD*) and surface quality of the joint, varying between about 30 (below which the rock is essentially rubble) and 100.

Essentially Eq. (3) provides adjustment factors to account for the properties of the jointed rock mass relative to intact blocks of rock. For pile construction, with relatively low damage and often in softer, e.g. carbonaceous, rocks, D may be assumed to be close to zero, and m_i in the range 3 to 10.

From the Hoek-Brown relationship in Eq. (2), the equivalent unconfined strength q_{ucs} and (bilateral) tensile strength q_t for the rock mass may be deduced by setting σ'_3 to zero to obtain $q_{ucs} = \sigma_{ci} s^a$ and setting $\sigma'_1 = \sigma'_3 = -q_t$ to obtain $q_t = s\sigma_{ci}/mb$. Hence the ratio of tensile to compressive strength is about $s^{0.5}/mb$. This ratio is often estimated as 0.1 for soft rock, although lower ratios are obtained for different combinations of s and m_b.

For pile design, where the rock is confined, it may be appropriate to consider what Hoek and Brown referred to as a 'global' rock mass strength σ_{cm}, allowing for confinement by stresses in the range from zero to $\sigma_{ci}/4$, expressed as

$$q_{cm} = \sigma_{ci} \frac{m_b + 4s - a(m_b - 8s)}{2(1+a)(2+a)(m_b/4 + s)^{1-a}} \quad (4)$$

The other important design parameter for rock is its modulus, generally expressed in terms of the Young's modulus. Liang et al. (2009) proposed a correlation (based on Bieniawski 1978), with the rock mass modulus E_m related to that of intact rock (E_i as measured in an unconfined compression test on an assumed undamaged sample) and the *GSI* by

$$E_m = \frac{e^{GSI/21.7}}{100} E_i \quad (5)$$

These various relationships are illustrated in Figure 2 for the case of zero damage (D = 0). It may be seen that the unconfined compressive strength ratio decreases exponentially, by a factor of 10 for each reduction in *GSI* by ~40, whereas the global mass strength ratio shows rather higher values for low and intermediate values of *GSI*.

Pile design parameters for soft rock are often correlated against the q_{ucs} so it is relevant to consider the ratio q_{ucs}/q_{cm}, which is the ratio of the unconfined compression strength measured in the laboratory to the in situ rock mass strength. That ratio is

plotted in Figure 3, showing that the true mass strength of rock increases to double the unconfined compression strength for GSI of 50%.

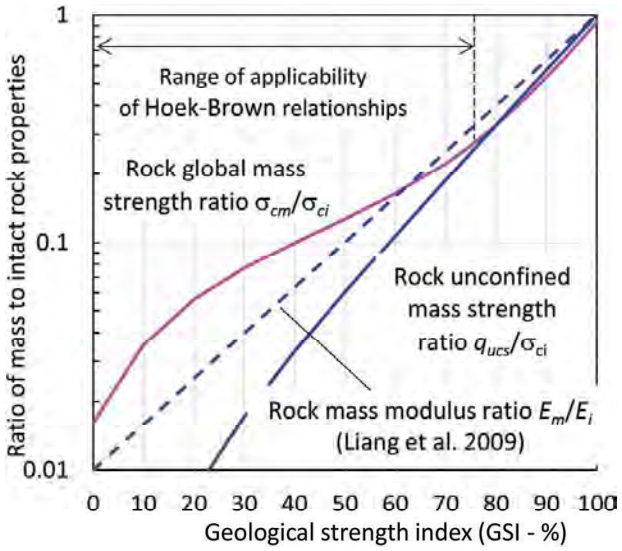

Figure 2. Ratios of mass to intact rock properties.

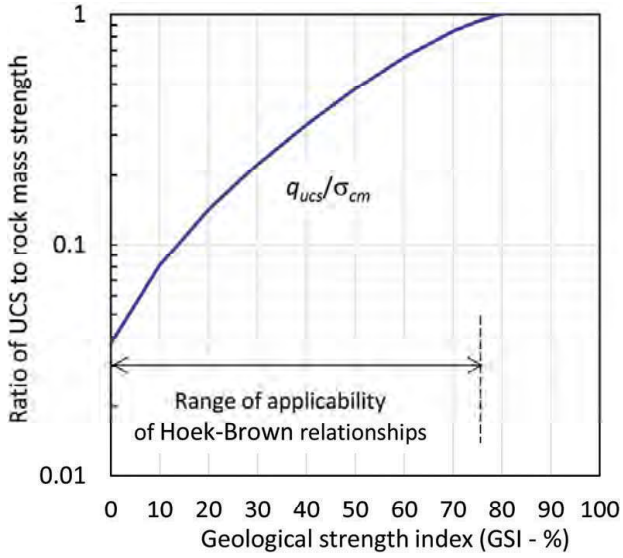

Figure 3. Ratios of mass to intact rock properties.

3 AXIAL PILE DESIGN PARAMETERS

3.1 *Construction effects*

Although the focus here is on jacked or driven piles, it is worth considering how design parameters might differ from the more common (in rock) construction technique of cast-in-situ rock sockets or grouted piles.

For the base resistance, mobilization of end-bearing capacity will require smaller displacements for jacked or driven piles (particularly the former) compared with a cast-in-situ pile. Figure 4 shows a bi-directional load cell developed by the Bolivian company Incotec, which can be lowered on the reinforcing cage prior to casting the pile. After curing of the pile the cell can be expanded to pre-load the pile base before it is finally grouted solid.

In principle, the reverse is likely to be true for the shaft resistance, with cast-in-situ piles offering higher shaft resistance due to interlocking effects, and hence dilation induced enhancement of the lateral effective stress as the pile is loaded, for cast-in-situ piles.

Figure 4. Expanded base pile construction.

Figure 5. Underreaming tool developed for Pluto project (https://www.lddrill.com/our-projects/pluto-jacket-installation/).

Figure 6. Expanded base pile construction.

As is discussed further below, in very weak rock (or strong soils) or very strong rock, the degree of interlocking for cast-in-situ piles may be small, requiring additional construction techniques in order to maximize shaft friction. Examples are shown in (a) Figure 5, where an underreaming tool was used to create grooves in the pile shaft for grouted insert piles constructed in high-quality limestone; and (b) Figure 6, which shows expandable 'lanterns' developed by Incotec and the construction process to expand them following casting of a pile, thus creating an elliptical expansion and enhanced load transfer between pile and soil. The concept is similar to the technology used for expanded base piles, patented in 1982 (Massarsch 2019).

Although the expanded base and shaft technology has generally been used in uncemented silts and sandy deposits, it would prove equally effective in ensuring robust load transfer for piles socketed into weak rock.

3.2 *Base resistance*

An extensive review of design approaches for the end-bearing resistance of piles in rock was given by Zhang & Einstein (1998). They documented a database of field measurements on piles from 0.3 m to 1.9 m diameter, for reported q_{ucs} values spanning from 0.6 MPa to 55 MPa. They proposed a non-linear fit to the data, expressed in non-dimensional form as

$$q_b = 15\sqrt{q_{ucs}p_a} \text{ or } \frac{q_b}{q_{ucs}} = \frac{15}{\sqrt{q_{ucs}/p_a}} \qquad (6)$$

where p_a is atmospheric pressure (0.1 MPa).

The above expression is shown with the database in Figure 7, together with what may be regarded as an upper bound design approach of $q_b/q_{ucs} = 5$.

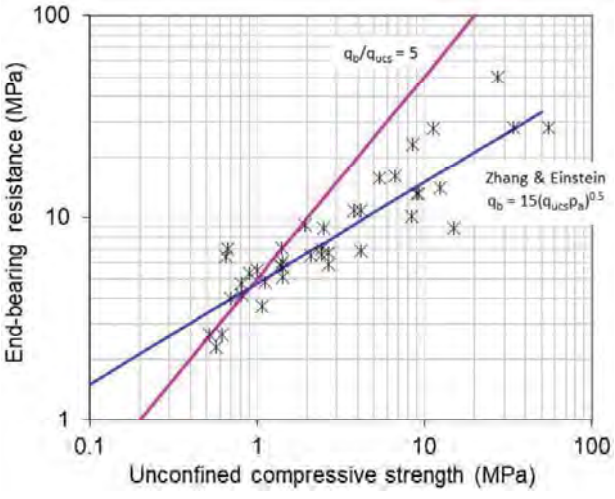

Figure 7. Zhang & Einstein (1998) database of pile base resistance in rock.

As indicated by (6), the Zhang & Einstein approach leads to very low 'bearing factors' in strong rock, which fall below unity for q_{ucs} values exceeding ~20 MPa. This does not seem reasonable physically, and may reflect vagaries in the UCS data, or limited base displacements in some cases.

An alternative hyperbolic variation of bearing factor $N_b = q_b/q_{ucs}$ may be expressed as

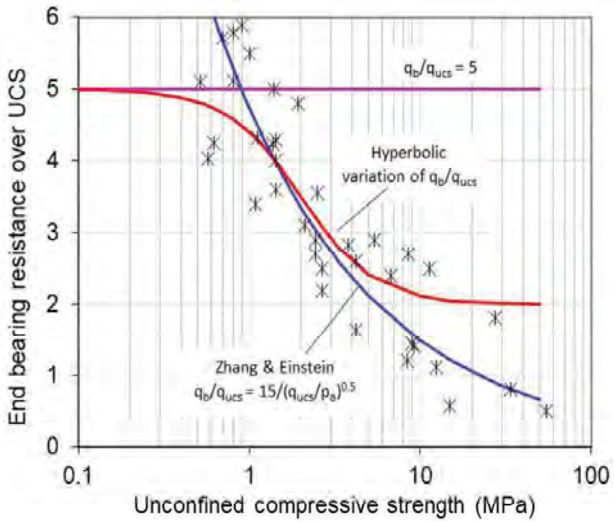

Figure 8. Hyperbolic variation of bearing factor shown with Zhang & Einstein (1998) database.

$$N_b = N_{b,\min} + \frac{\left(N_{b,\max} - N_{b,\min}\right)}{1 + \left(q_{ucs}/q_{ucs,ref}\right)^2} \qquad (7)$$

taking $N_{b,min}$ as 2, $N_{b,max}$ as 5 and a reference UCS value of $q_{ucs,ref} = 2$ MPa. This is shown in Figure 8.

Since the end-bearing response of piles is closely linked to cavity expansion, the reduction in bearing factor for increasing rock strength is consistent with the stiffness of rock being a non-linear multiple of rock strength, reducing with increasing strength.

Although the Zhang & Einstein database was developed for cast-in-situ piles, it is also applicable to jacked or driven piles. Assessment of the rock quality and strength is critical. As a guide, Stevens et al. (1982) comment that refusal of driven piles will generally occur in rock with UCS exceeding 5 MPa. Also, if piles are to be driven a significant distance into the rock, consideration should be given to potential tip damage and premature refusal. Careful monitoring of hammer energy and blowcount is needed, ideally with stress-wave monitoring as well, in order to minimize risk of over-stressing the pile tip (Wiltsie et al. 1985). Also, as discussed later, the potential for hard inclusions such as boulders or unweathered clumps of rock to dent the tip of open-ended pile needs to be assessed.

3.3 *Shaft resistance*

The shaft friction of cast-in-situ piles relies heavily on interlocking between the pile and surrounding rock (Seidel & Haberfield 1995). The resulting magnitude of shaft friction is a function of the height and roughness angle of the rock asperities created by drilling, which tend to reach a maximum in rock of intermediate strength (q_{ucs} of ~2 MPa) but reduce significantly for high strength rock (Figure 9a).

This leads to a relationship for the ratio of shaft friction to the rock shear strength expressed as

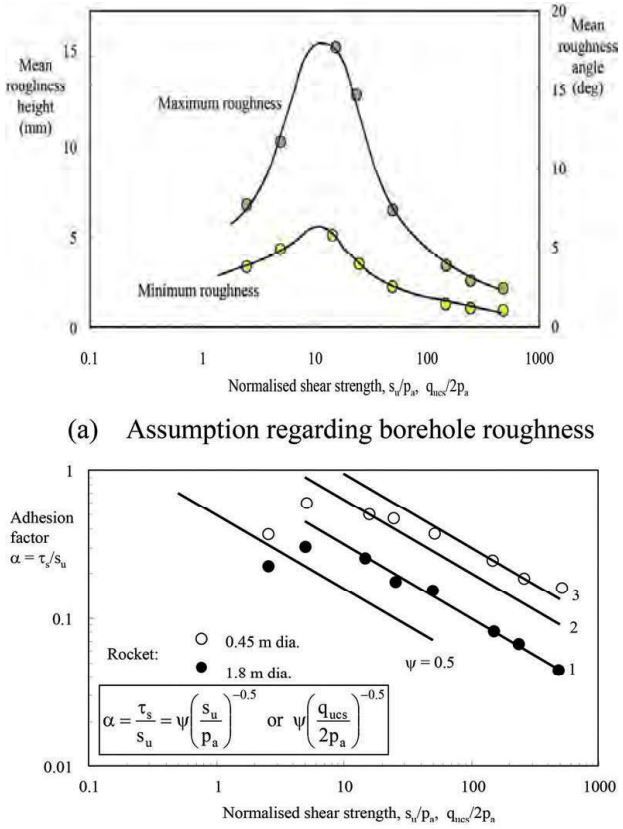

Figure 9. Predictions of rock-socket shaft friction from ROCKET (Seidel & Haberfield 1995).

$$\frac{\tau_s}{(q_{ucs}/2)} = \frac{\psi}{\sqrt{q_{ucs}/2p_a}} \text{ or } \tau_s = \psi\sqrt{\frac{q_{ucs}}{2}p_a} \qquad (8)$$

illustrated in Figure 9b. As evident from this figure, there is also an effect of the pile diameter (assuming that the rock asperity heights are independent of diameter), with reducing effect of dilation as the diameter increases.

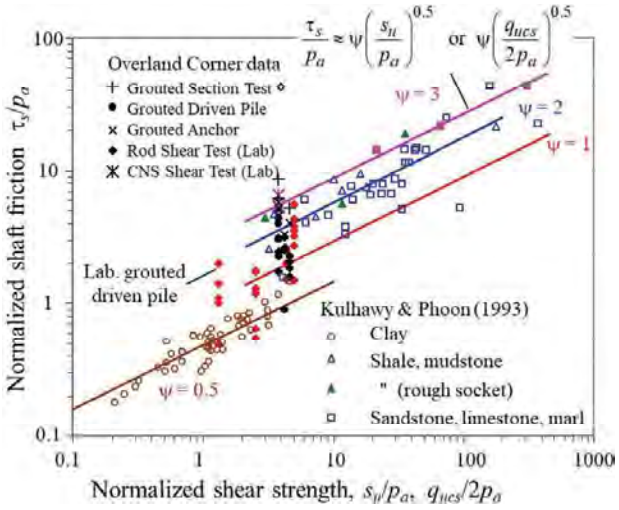

Figure 10. Variation of shaft friction with rock shear strength (extended from Kulhawy & Phoon 1993).

The power law variation of τ_s/q_{ucs} with rock strength is consistent with the data assembled by Kulhawy & Phoon (1993) shown in Figure 10, supplemented by data from field tests (Randolph et al. 1996). The bulk of the data for rock follow the trend line for $\psi = 2$, which is equivalent to $\tau_s = 0.45 q_{ucs}{}^{0.5}$, using units of MPa.

In weak rock, where cone penetration testing is possible, the shaft friction for cast-in-situ piles may also be correlated with the cone resistance. Consistent with the trend for τ_s/q_{ucs}, the ratio of shaft friction to cone resistance reduces with increasing q_{cone}, with a trend of (Randolph et al. 1996)

$$\frac{\tau_s}{q_{cone}} \approx 0.02 + 0.2e^{-0.04 q_{cone}/p_a} \qquad (9)$$

In most cases the lower limit of τ_s of about 2% of the cone resistance will apply.

The mineralogy of a given rock may be expected to have a much greater effect on the shaft friction for jacked or driven piles than for cast-in-situ piles. For example, in carbonate material the process of pile driving creates an annulus of completely destructured material adjacent to the pile, which leads to very low shaft friction for piles driven into limestone and also, prior to set up, in chalk. Typical design values of shaft friction for weak limestone are in the range 5 to 15 kPa unless site specific test data are available that can justify higher values. Indeed, higher values of shaft friction are appropriate for some of the carbonate soils in the Middle East, particularly where calcium carbonate content falls below 70 % (Thomas et al. 2010).

In chalk, however, although shaft friction during pile installation is similarly low, with destructured

'puttied' chalk adjacent to the pile, relatively strong setup is observed, potentially by a factor of five or more (Dürhkop et al. 2015; Ciavaglia et al. 2017; Buckley et al. 2018). During installation, shaft friction is typically around 15 to 25 kPa apart from near the pile tip where values as high as 200 kPa may be reached. The long-term shaft friction after set up may reach 150 kPa or more, but for design purposes is often limited to 100 kPa (Augustesen et al. 2015).

For non-carbonate rocks such as mudstones, much higher values of shaft may be achieved, although there are rather limited data from full scale tests. Design approaches vary from treating the rock as a strong clay, following American Petroleum Institute design guidelines (API 2011), or using empirical correlations based on test data. For the former, and assuming strength ratios (s_u/σ'_{vo}) exceeding unity, the shaft friction would vary as

$$\tau_s = 0.5\sigma'^{0.25}_{v0}(q_{ucs}/2)^{0.75} \qquad (10)$$

Terente et al. (2017) showed that this can be very conservative, based on shaft friction values deduced from dynamic load tests, which were well in excess of 500 kPa at depths of 15-25 m below seabed in rock with q_{ucs} values of 1-2 MPa. The shaft friction values also tended to increase with depth, suggesting that an effective stress approach based on estimated in situ horizontal effective stresses might be more appropriate.

In summary, shaft friction for piles jacked or driven into rock varies significantly with the mineralogy of the rock and the extent to which (a) it is destructured and undergoes compaction during pile installation, and (b) physiochemical processes that may lead to time-dependent recovery of structure and strength. Data from full-scale testing, including monitoring of piles during installation, is needed in order to reduce the level of conservatism necessary in its absence.

4 TRENDS IN OFFSHORE WIND INDUSTRY AND PILE TIP DAMAGE

4.1 *Introduction*

The offshore wind industry has relied heavily on the use of large diameter so-called 'monopiles' to support offshore wind turbines. To date, developments have been concentrated in Europe, in the heavily glaciated dense sands and overconsolidated clays such as found in the North Sea. As the industry now expands into North America and Asia, more varied and less competent sediments are encountered, which have increased design challenges.

Typical monopile diameters have increased gradually over the last two decades, in response to the increase in generating power and size of the wind turbines (see Figure 11). Diameters have now reached 8 to 10 m, with diameter to wall thickness (D/t) ratios generally exceeding 80 and sometimes greater than 110.

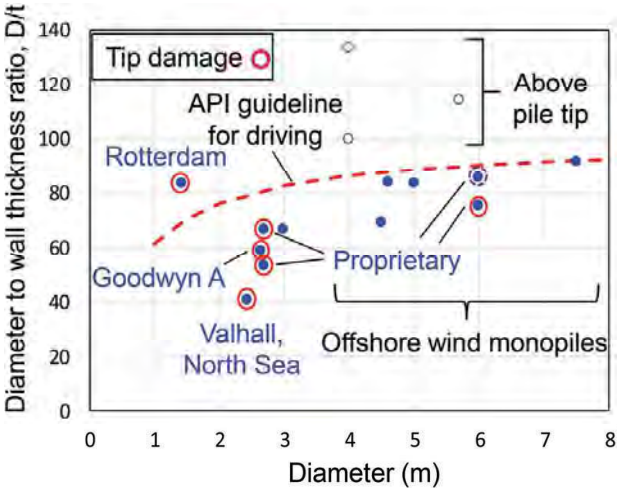

Figure 11. Trends for diameter and D/t in offshore wind industry and incidents of pile tip damage.

The combination of more challenging sediments and increased diameter and D/t ratios has made the piles more vulnerable to tip damage. This may originate from minor fabrication imperfections such as out of roundness, or from asymmetric loading of the pile tip as it is penetrated through sediments containing boulders or other localized hard zones.

A rather extreme case of such damage was reported by Broos et al. (2017) from piles extracted during the expansion of Rotterdam Harbour (Figure 12. The piles had originally been installed by driving at a rake of 1 in 5, to penetrate medium to dense sands with cone resistance of 25 to 40 MPa. It is possible that the raking angle (around 11 degrees) contributed to the distortion, since the pile tip would have encountered any stronger stratum at one edge.

Figure 12. Pile tip damage from Rotterdam harbour.

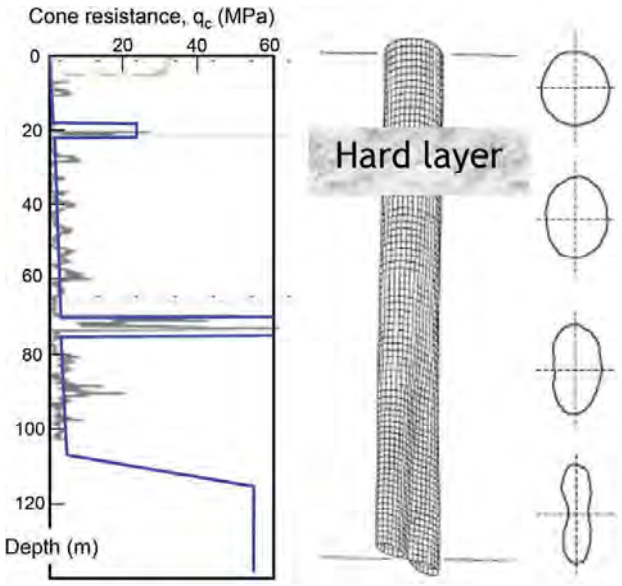

Figure 13. Soil strength profile and measured growth in pile distortion at Goodwyn.

Although initial damage to a pile tip may be relatively minor, once the pile tip cross-section is no longer circular, either because of an originally elliptical shape or a minor dent, the soil can act as a dye, with the pile 'extruding' through the soil following the current shape of the tip. This type of failure occurred for Woodside's Goodwyn platform on the North-West shelf of Australia as a result of driving 2.65 m diameter piles through a 5 m thick layer of strong calcarenite (cone resistance estimated as ~80 MPa), as shown in Figure 13 (Erbrich et al. 2010).

The process of extrusion buckling is very challenging numerically because of the extreme geometric and material non-linearities. Barbour & Erbrich (1995) developed an ABAQUS-based analysis procedure called BASIL to address this, using a system of pile-soil interaction springs attached at nodes to the 3-dimensional model of the pile, avoiding the need to model the soil continuum explicitly. An example outcome of a BASIL analysis is shown in Figure 14.

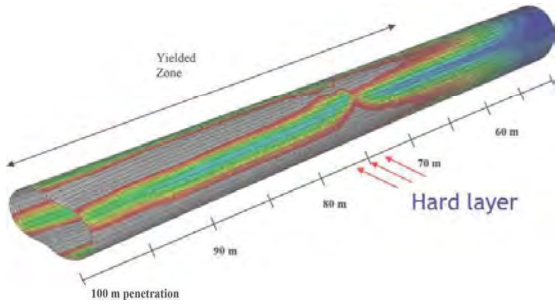

Figure 14. Example pattern of plastic strains for a pile pushed 25 m beyond the hard layer.

Doctoral research being undertaken at UWA by Juliano Nietiedt has resulted in quantitative guidelines to estimate the potential for (a) inelastic denting of a pile tip as a result of boulder impact, and (b) propagation and growth of a small dent by extrusion buckling. The work combines data from centrifuge model tests (Nietiedt et al. 2020) and numerical modelling. The results presented below are preliminary findings that are in the process of being submitted as journal publications (Nietiedt et al. in prep a,b,c).

4.2 *Pile tip damage from boulder impact*

Pile tip damage can be initiated by contact with a sloping hard layer or a localized zone of strong material such as a boulder or unweathered rock, as illustrated in Figure 15. Large deformation three dimensional (3D) finite element analyses were undertaken in which an embedded was forced downward under an imposed vertical displacement, meanwhile being allowed to rotate freely. The ellipsoidal boulder was characterized by the long and short axis dimensions, $a_{boulder}$ (or a_b) and $b_{boulder}$ (or b_b) and the contact point by an eccentricity e_b.

Figure 16 Shows typical vertical and horizontal reaction curves for the worst value of eccentricity e_b/a_b = 0.3. The reactions are normalized by the cone resistance established by separate numerical analyses of cone penetration and also by the maximum cross-sectional area of the boulder A_{pi}.

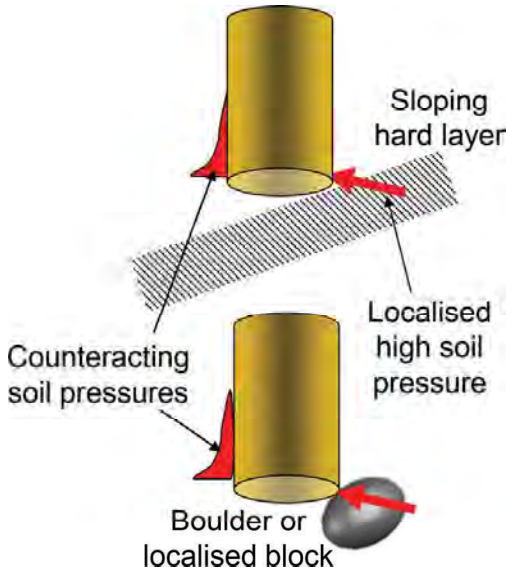

Figure 15. Initiation of damage by localized contact with hard material.

The maximum horizontal reaction force can be compared with the horizontal force F_p required to cause plastic deformation of the pile tip. This force may be expressed as

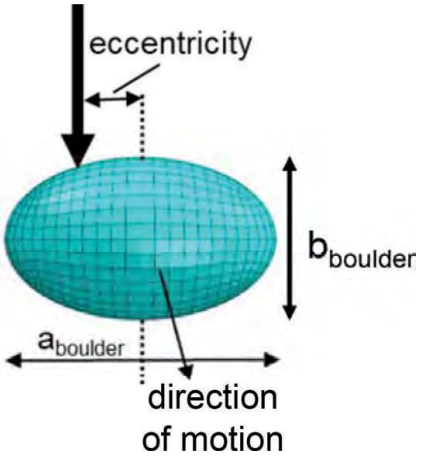

Figure 16. Simplified modelling of boulder impact.

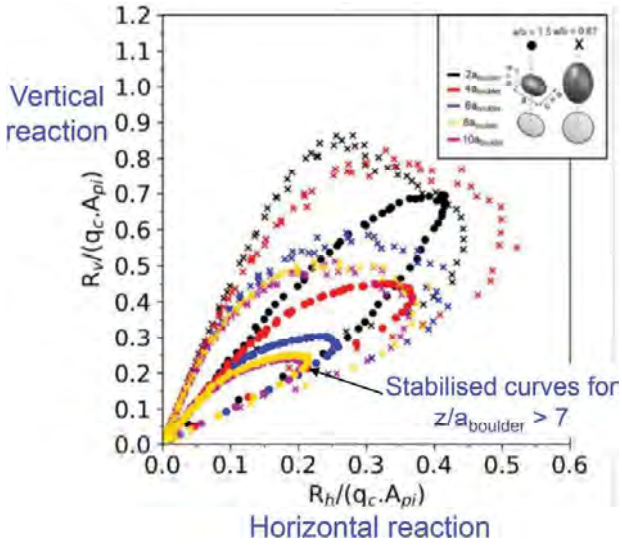

Figure 17. Reaction curves for simplified 3D finite element analyses of boulder impact.

$$\frac{F_p}{f_y t^2} \approx 0.25 \left(\frac{s_{load}}{t}\right)^{0.4} \qquad (11)$$

where f_y is the yield stress of the steel, t is the pile wall thickness at the tip and s_{load} is the length of the line load applied to the pile to deform it.

The value of $F_p/f_y t^2$ varies between 0.5 and 1.2 as s_{load}/t ranges between 5 and 40. The coefficient may be compared with the value of 1.2 proposed by HSE (2001).

4.3 *Conditions for extrusion buckling*

Conditions for extrusion buckling may be assessed by considering the forces imposed on the pile as it advances into the soil. Consider first an idealized slightly ellipsoidal deformation of the pile tip, leading to a trumpet shape on one vertical plane through the pile axis, and a slight inward taper on the orthogonal plane (see Figure 18). As the pile advances, external lateral pressure will build up on the outside of the tapered profile and, to a lesser degree, internal lateral stresses will increase within the trumpet profile. The key geometric detail is the angle that the inwardly tapered wall makes with the pile axis. The greater that angle, the larger will be the buildup of lateral soil pressure – essentially a feedback process that encourages further growth of the pile deformations.

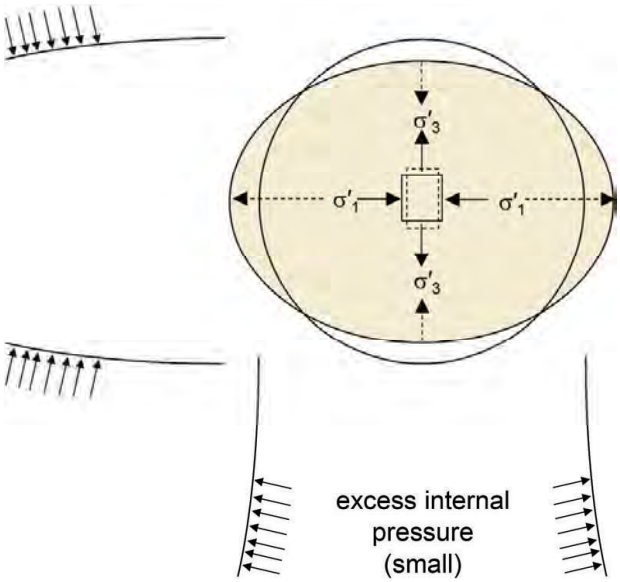

Figure 18. Feedback loop of stress changes due to elliptical deformation of the pile tip.

Laboratory testing of thin-walled piles, with D/t of 50 and 100, allowed the shape of asymmetric dents at the pile tip to be parameterized. Figure 19 shows how a dent may be quantified by the maximum departure δ from the original circular shape, the chord width w and the length s_{dent} along the length of the pile. The figure also indicates the expected gradual buildup of external soil pressure as the pile is penetrated. This starts from zero at the pile tip as the pile cuts into fresh soil.

Numerical analysis allowed evaluation of the resulting soil pressure, as indicated in Figure 20.

It is then necessary to quantify the effect of the increasing soil pressure on the structural response of the pile, which gradually weakens as the magnitude of the dent increases. As indicated in Figure 21, the reloading stiffness reduces as the dent grows, while the force F to cause additional plastic deformation increases but trends towards a plateau. The subscripted F_p and δ_p refer to the force and dent magnitudes that first cause plasticity in the pile.

Eventually, the results of boulder impact and conditions for extrusion buckling may be combined to allow estimation of the overall pile response. If the pile tip impacts a sufficiently large boulder at only

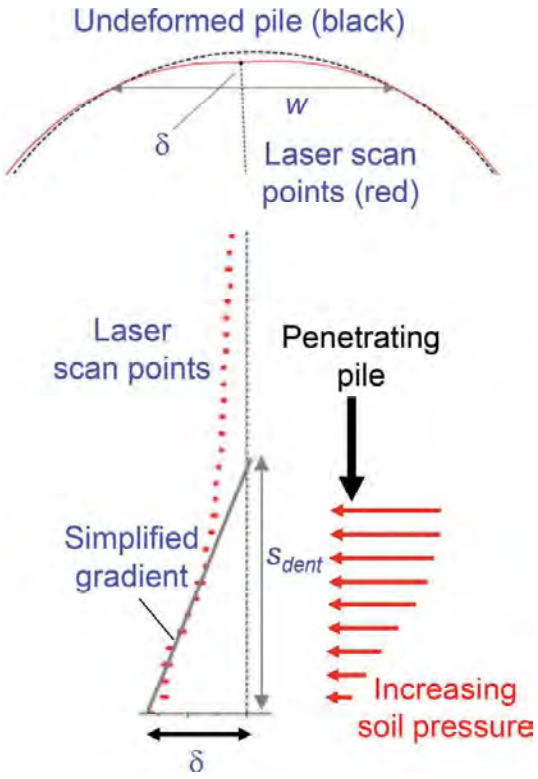

Figure 19. Dent shape and indicative soil pressures.

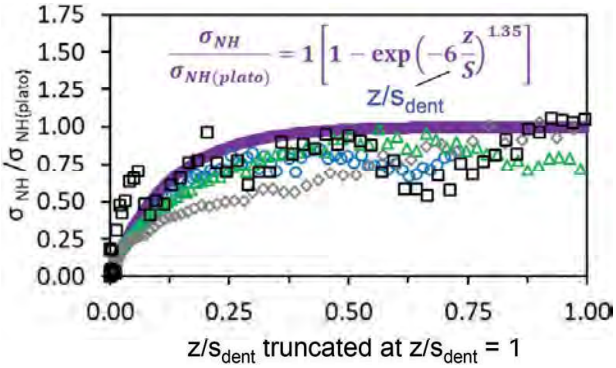

Figure 20. Evolution of external soil stress along the length of the pile.

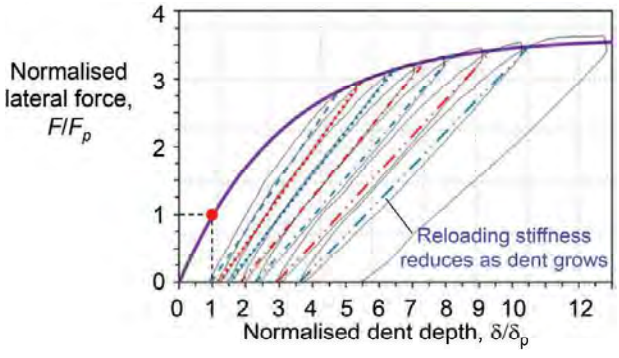

Figure 21. Evolving structural response of the pile.

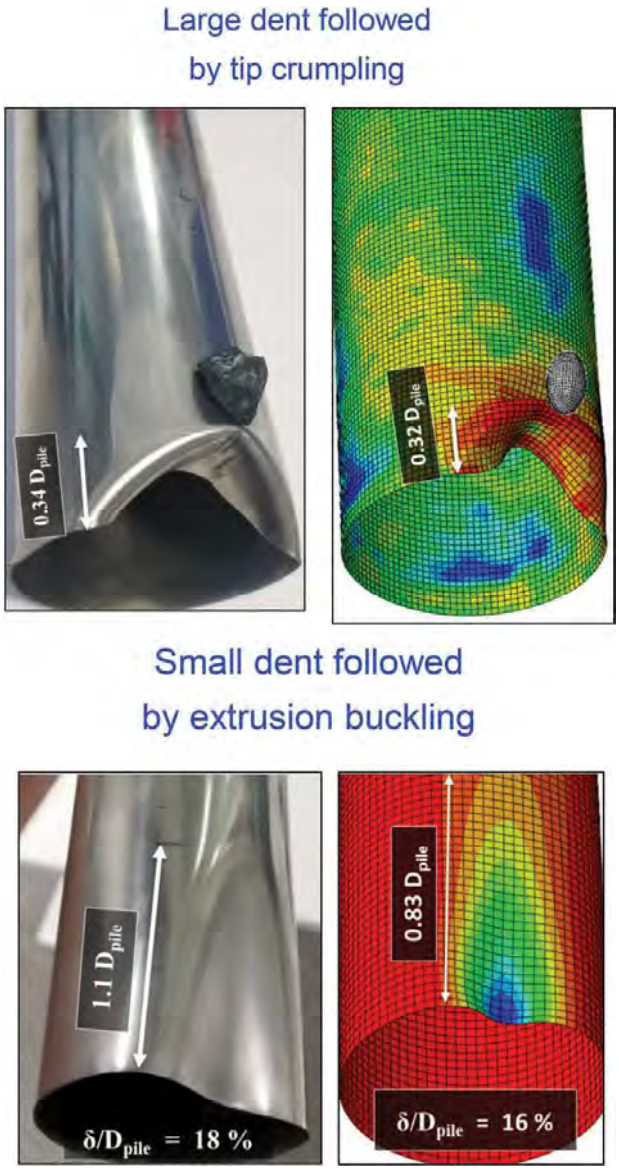

Figure 22. Comparison of pile shapes from centrifuge model tests (left) and 3D finite element analyses.

a small eccentricity, the impact force is likely to exceed significantly the force to cause plasticity (assuming that the boulder is embedded in reasonably strong soil). In that case a large dent will eventuate, as evidenced from both physical and numerical modelling (upper part of Figure 22).

Alternatively, if the pile tip hits a boulder near the edge, or the surrounding soil is less strong, only a small (or no) dent will eventuate. However, that dent may grow through extrusion buckling as the pile is penetrated further (lower part of Figure 22).

Although the predictive framework is still being developed (Nietiedt et al., in prep. a,b,c), preliminary comparisons with experimental and numerical results shows reasonably good agreement, as shown in Figure 23.

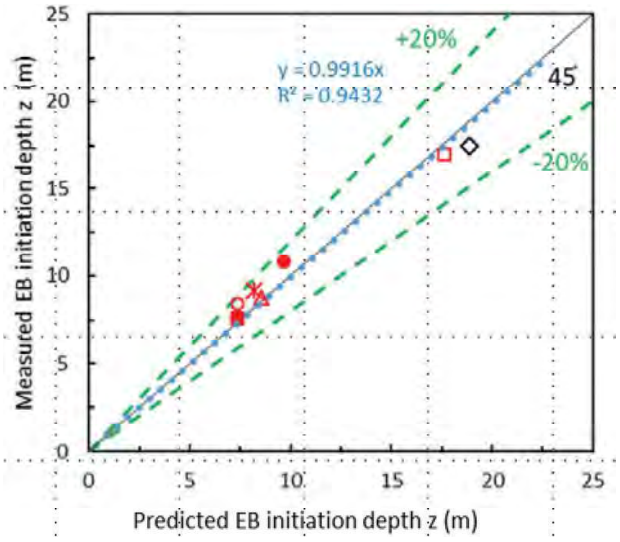

Figure 23. Comparison of predicted and measured depths to initiate extrusion buckling.

4.4 *Alternative approaches for OWF foundations*

Alternative foundation types are being explored by the wind industry for conditions that are not conducive to large diameter monopiles. The most common alternative is the use of a jacket structure to support the wind turbine, with the structure itself supported on smaller diameter driven piles or suction caissons.

Recently, one of the major offshore installers (Heerema) publicized alternative 'silent' foundation approaches including screw piles and hydraulically jacked piles using a similar approach to Giken's Silent Piler. The Heerema technique is illustrated in Figure 24.

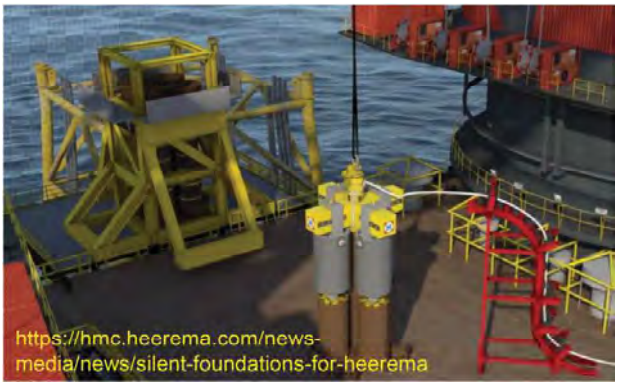

Figure 24. Heerema's silent piling technique using small group of jacked piles.

This development raises the issue of other substitute arrangements for large diameter monopiles, such as that illustrated in Figure 25. The monopile is replaced by a ring of smaller piles, grouted (after installation) into a transfer template that links the turbine tower to the pile group. Such an arrangement, which requires rather less steel than the monopile for a given rotational stiffness, lends itself to push-in technology.

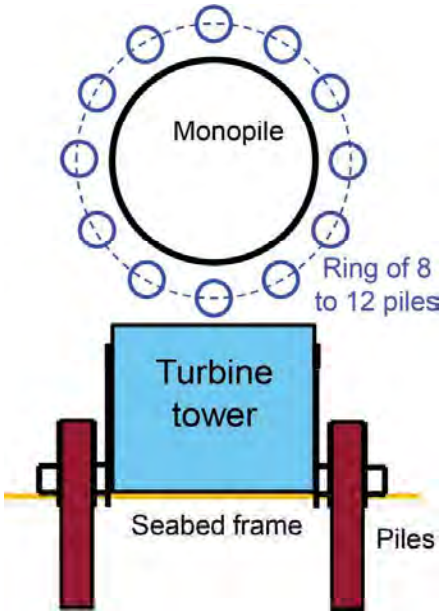

Figure 25. Replacement of large diameter monopile by ring of smaller piles.

5 CONCLUDING REMARKS

This paper has explored design challenges for jacked and driven piles in strong soil and weak rock, both for general application and with respect to the expanding offshore wind industry. Approaches for characterizing the strength of soft rock and correlations for pile design parameters were summarized, considering the effect of differences in construction.

The offshore industry routinely uses steel pipe piles, in particular large diameter relatively thin-walled monopiles. These are vulnerable to tip damage and extrusion buckling during installation. Background to such type of damage was discussed. Preliminary results from current doctoral research were presented, aimed at developing a quantitative framework to predict the potential for tip damage from either boulder damage or extrusion buckling of an out-of-cylindrical thin-walled pile.

Alternative foundation concepts that might lend themselves to 'silent piling' were discussed briefly, with a monopile replaced by a group of smaller piles, either clustered together or in a ring.

REFERENCES

API 2011. *Recommended Practice 2GEO: Geotechnical and Foundation Design Considerations, 1st*Ed. American Petroleum Institute, Washington, DC.

Augustesen, A.H., Leth, C.T., Østergaard, M.U., Møller, M., Dührkop, J. & Barbosa, P. 2015. Design methodology for cyclically and axially loaded piles in chalk for Wikinger OWF. *Proc. Int. Symp. Frontiers in Offshore Geotechnics III*. Taylor & Francis, London, 509–514.

Barbour, R. & Erbrich, C.T. 1995. Analysis of soil skirt interaction during installation of bucket foundations using ABAQUS. *Proc. Of ABAQUS Users Conference*, Paris.

Bieniawski, Z.T. 1978. Determining rock mass deformability: Experience from case histories. *Int. J. Rock Mech. Min. Sci. Geomech. Abstr.*, 15:237–248.

Broos, E., Sibbes, R. & de Gijt J. 2017. Widening a harbor basin, demolition of a deep see quay wall in Rotterdam. *Proc. of COME2017: Decommissioning of Offshore Geotechnical Structures*, Hamburg, Germany, 251–262.

Buckley, R.M., Jardine, R.J., Kontoe, S., Parker, D. & Schroeder, F.C. (2018). Ageing and cyclic behaviour of axially loaded piles driven in chalk. *Géotechnique*, 68 (2),146–161.

Ciavaglia, F., Carey, J. & Diambra, A. 2017. Time-dependent uplift capacity of driven piles in low-to-medium-density chalk. *Géotechnique Letters*, 7(1): 1–7.

Dührkop, J., Augustensen, A.H. & Barbosa, P. 2015. Cyclic pile load tests combined with laboratory test results to design offshore wind turbine foundations in chalk. *Proc. Int. Symp. Frontiers in Offshore Geotechnics III*. Taylor & Francis, London, 533–538.

Erbrich, C.T., Barbosa-Cruz, E. & Barbour, R. 2010. Soil-pile interaction during extrusion of an initially deformed pile. *Proc. of 2nd International Symposium on Offshore Geotechnics*, Perth, 489–494, Taylor & Francis, London, Australia.

Hoek, E. & Brown, E.T. 1997. Practical estimates of rock mass strength. *Int. J. Rock Mech. Min. Sci*. 34(8): 1165–86.

Hoek, E., Carranza-Torres, C.T. & Corkum, B. 2002. Hoek-Brown failure criterion - 2002 edition. *Proc. 5th North American Rock Mech. Symp*., Toronto, Canada.

HSE 2001. *A Study of Pile Fatigue During Driving and In-Service and of Pile Tip Integrity*. Offshore Technology Report 2001/018, Health and Safety Executive, UK, published by Her Majesty's Stationery Office, Norwich.

Kulhawy, F.H. & Phoon, K.K. 1993. Drilled shaft side resistance in clay soil to rock. *Geotech. Spec. Pub. No. 38, Design and Performance of Deep Foundations*, ASCE, New York, 172–183.

Liang, R., Yang, K. & Nusairat, J. 2009. P-y criterion for rock mass. *J. Geotech. & Geoenviron. Eng*., ASCE, 135 (1): 26–36.

Massarsch, K.R. 2019. The evolution of the expander body concept and future applications. Keynote Lecture, *Proc. 4th Int. Congress of Deep Foundations of Bolivia*. [https://www.cfpb4.com/]

Nietiedt, J.A., Randolph, M.F., Gaudin, C., Doherty, J.P., Kallehave, D., Gengenbach, J. & Shonberg, A. 2020. Physical modelling of pile tip damage arising from impact driving. *Proc. 4th Int. Symp. on Frontiers in Offshore* Geotechnics, *ISFOG2020*, Austin, Deep Foundations Institute, Hawthorne, USA, 787–797.

Nietiedt, J.A., Randolph, M.F., Gaudin, C. & Doherty, J.P. In prep. a. Numerical assessment of tip damage during pile installation in boulder rich soils. In preparation.

Nietiedt J.A., Randolph M.F., Gaudin C. Doherty J.P. In prep. b. Centrifuge model tests investigating initiation and propagation of pile tip damage during driving. In preparation.

Nietiedt J.A. Randolph M.F., Gaudin C. & Doherty J.P. In prep. c. Calculation approach for initiation of extrusion buckling of steel pipe piles. In preparation.

Randolph, M.F. 2019. Considerations in the design of piles in soft rock. Keynote paper. *Proc. Int. Conf. on Geotechnics for Sustainable Infrastructure Development*, Hanoi.

Randolph, M.F., Joer, H.A., Khorshid, M.S. & Hyden, A.M. 1996. Field and laboratory data from pile load tests in calcareous soil. *Proc. 28th Annual Offshore Tech. Conf*., Houston, OTC 7992, 1: 327–336.

Seidel, J. & Haberfield, C.M. 1995. The axial capacity of pile sockets in rocks and hard soils, *Ground Engineering*, 28(2): 33–38.

Stevens, R.S., Wiltsie, E.A. & Turton, T.H. 1982. Evaluating pile drivability for hard clay, very dense sand, and rock. *Proc. 14th Annual Offshore Tech. Conf*., Houston, OTC 4205:465–469.

Terente, V., Torres, I., Irvine & Jaeck, C. 2017. Driven pile design method for weak rock. *Proc. 8th Int. Conf. Offshore Site Investigation and Geotech*., Society for Underwater Technology, London, 1: 652–657.

Thomas, J., van den Berg, M., Chow, F. & Maas, N. 2010. Behaviour of driven tubular steel piles in calcarenite for a marine jetty in Fujairah, United Arab Emirates. *Proc. Int. Symp. on Frontiers in Offshore Geotechnics*, Perth, Taylor & Francis, London, 549–554.

Wiltsie, E.A., Stevens, R.F. & Vines, W.R. 1985. Pile installation acceptance in strong soils. P*roc. 2nd Int. Conf. on Application of Stress Wave Theory on Piles*, Balkema, Stockholm, 72–78.

Zhang, L. & Einstein, H.H. 1998. End bearing capacity of drilled shafts in rock, *J. Geot. & Geoenviron. Eng*., ASCE, 124(7): 574–584.